Experimental and Mathematical Modeling Studies of the Separation of Zinc Blende and Wurtzite Phases of CdS Nanorods by Density Gradient Ultracentrifugation

Xiuju Ma,[†] Yun Kuang,[†] Lu Bai, Zheng Chang, Feng Wang,* Xiaoming Sun,* and David G. Evans

State Key Laboratory of Chemical Resource Engineering, Box 98, Beijing University of Chemical Technology, Beijing 100029, People's Republic of China. [†] Contributed equally to this work.

ABSTRACT Identifying the phase purity of CdS nanorods (NRs) is complicated by the serious overlap between the X-ray diffraction peaks of zinc blende and wurtzite phases as well as anisotropic growth, which might hide a mixed phase. Here we show that the density gradient ultracentrifugation rate separation method can be used to sort CdS NRs synthesized under nitrogen according to differences in particle size and morphology. Furthermore, it was found that the different sized NRs formed in a single batch synthesis had different phases: the thinner ones (<3.5 nm in diameter) were predominantly wurtzite phase, while the thicker ones (>5 nm in diameter) were mainly zinc blende phase. Dark-field transmission electron microscopy (TEM) and high-resolution TEM images indicated the presence of numerous stacking faults in the thick zinc blende rods, while the wurtzite thin rods were exclusively single crystals. As a result of the differences in phase and stacking faults, the NRs showed different photoluminescent properties. The development of an effective way of separating such NRs thus leads to further insight into the differences in phase, structure, and optical properties between individual colloidal particles synthesized in a single batch. A preliminary mathematical model of the separation process has been proposed.

KEYWORDS: nanoseparation · quantum rods · aspect ratio · CdS · crystal phase

One-dimensional semiconductor nanoparticles have attracted vast attention due to their intrinsic dimension-dependent optical and electrical properties,[1−3] which have made them ideal building blocks in areas such as solar cells,[4] biological labels,[5,6] light-emitting diodes,[7−9] electronics,[10] and lasers.[11,12] In the case of nanorods (NRs), an ideal sample should not only exclude particles with other structures (such as nanospheres or nanobelts[14,15]) but also have particles with a narrow distribution of diameter and length, and high phase purity. CdS NRs have been widely studied,[16−20] but syntheses usually yield batches of CdS NRs with a wide distribution of length and diameter. Even worse, even when all the particles are rod-shaped, there may be two phases, zinc blende (ZB) and wurtzite, coexisting in a single batch. It is often difficult to obtain conclusive evidence for this, because the (111), (220), and (311) X-ray diffraction (XRD) peaks of the ZB phase are located at the same positions as the (002), (110), and (112) peaks of the wurtzite phase. The distinctive (200) peak of the ZB phase is often too weak to be observed since it is obscured by the stronger diffraction peaks nearby (e.g., (002) of wurtzite phase or (111) of ZB), especially when nanosize causes a significant broadening of the XRD peaks. Another distinctive peak of the ZB phase located at ~80° 2θ (for Cu Kα radiation) has generally not been considered in previously published XRD patterns.[15,21−23] Identifying the phase purity is further complicated by the anisotropic growth of the wurtzite structure along the *c* axis, leading to very strong (002) diffraction peaks that overlap with the (111) diffraction peak of the ZB structure.

The density gradient ultracentrifugation rate separation (DGURS) method has emerged as an efficient tool for the separation of nanoparticles with different compositions and morphologies.[24−29] The discriminative separation of nanostructures (i.e., nanoseparation) has been used to sort colloidal particles according to differences in size and structure and has led to new insights into structure−property relationships and mechanisms of formation of nanoparticles.[26,28] For instance, we have identified the relationship between size and composition for FeCo@C nanoparticles.[29] Very recently we developed a O_2-manipulated synthesis method inspired by sorting CdS NRs synthesized in air.[30]

* Address correspondence to sunxm@mail.buct.edu.cn; wangf@mail.buct.edu.cn.

Received for review January 29, 2011 and accepted March 1, 2011.

Published online March 01, 2011
10.1021/nn200374t

In this report, we describe how CdS NRs synthesized in a N_2 atmosphere can be sorted using the DGURS method and a study of the structure, phase, morphology, and photoluminescence properties of the different fractions. Finally a mathematical model of the separation process has been proposed.

RESULTS AND DISCUSSION

Solvothermal synthesis of CdS NRs followed the method reported in the literature,[21] and the final products were dispersed in cyclohexane for characterization and separation. Figure 1A shows a transmission electron microscopy (TEM) image of as-prepared CdS NRs, which indicates that the sample contained rods with varied length and length-to-diameter ratio (aspect ratio). Interestingly, the short rods were usually thick, with aspect ratios of 1.4−1.8, while the long ones were usually slim, with aspect ratios of 3.4−3.9.

The as-prepared NRs were characterized by X-ray diffraction (XRD), as shown in Figure 1B. The three strongest peaks, located at 26.5°, 44°, and 52° 2θ (Cu Kα radiation), can be indexed to either the (111), (220), and (311) reflections of the ZB phase CdS (cubic structure, JCPDS 10−0454, located at 26.51°, 43.96°, and 52.13°, respectively, in the standard data, labeled in red) or the (002), (110), and (112) reflections of wurtzite phase CdS (hexagonal structure, JCPDS 41−1049, located at 26.51°, 43.68°, and 51.82°, respectively, in the standard data, labeled in black). A weak shoulder peak at ∼30° could be indexed to the (200) reflection of a ZB phase, but could also possibly be due to broadened (101) or (002) peaks of a wurtzite phase. A very weak peak at ∼64.0° 2θ may correspond to the distinctive (400) peak of ZB, but its intensity is too low to make a definite assignment. The distinctive (103) peak (at 47.8° 2θ) of the wurtzite phase clearly indicates the presence of this phase, but its rather low intensity relative to those of the two peaks nearby (44° and 52° 2θ characteristic of both ZB and wurtzite phases) suggests the presence of both phases. On balance, the XRD data suggest the presence of both ZB and wurtzite phases, but do not confirm this unambiguously. If two phases are present, an even more challenging question arises: do the two phases coexist in one individual NR or are individual NRs phase pure? Furthermore, if the latter is the case, it would be interesting to know whether the two phases were formed concurrently or consecutively in the synthesis process. These questions can be answered only after nanoseparation of the mixture, however.

Density gradient ultracentrifugation rate separation of the CdS NRs was performed[28] using a five-layer density gradient (made with 30%, 40%, 50%, 60%, and 70% cyclohexane/CCl_4 solutions, as shown in Figure 2A) and centrifugation at 30 000 rpm (relative centrifugal force, RCF = 113600*g*) for 70 min (the photo of vessel "a" was taken before centrifugation, and that of "b" was taken after centrifugation). Under 365 nm UV light irradiation, the colors of the fractions in the centrifuge tube varied from blue to green with increasing fraction number (Figure 2A, tube "c").

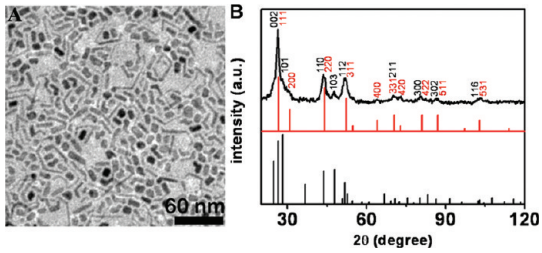

Figure 1. (A) TEM image of CdS NRs; (B) XRD patterns of as-prepared CdS NRs and standard data for the zinc blende phase (in red) and the wurtzite phase (in black) of CdS.

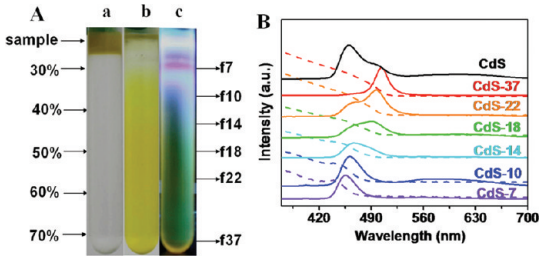

Figure 2. (A) Digital camera images of the ultracentrifuge tubes before and after separation at 30 000 rpm: (a) before separation; (b) after centrifugation for 70 min; (c) separated NRs under 365 nm UV irradiation (fX means the Xth fraction going from top to bottom). (B) Photoluminescence (solid lines) and absorbance spectra (dotted lines) of typical fractions after separation (the black line shows the photoluminescence spectrum of the CdS product before separation).

The UV photoluminescence (PL) spectra (with excitation at 360 nm) of the separated fractions are shown in Figure 2B. Bulk CdS is a semiconductor with a band gap of 2.4 eV, corresponding to band-edge emission at ∼510 nm. Most of the NR fractions (e.g., f7−f22 in Figure 1B) showed blue-shifted band-edge emission (455−500 nm), characteristic of particles in the quantum-confined size regime.[31,32] However those located at the very bottom (e.g., f37 in Figure 1B) had essentially the same photoluminescence properties as bulk CdS. The gradual red-shift of the band-edge emissions with increasing fraction number (Figure 2B) implies that the particles in the fractions lower down the tube are larger than those in the upper part of the tube, as we have seen in previous separations of CdSe[33] and CdS[30] NRs. It is interesting to see f10 was the only fraction showing surface trap state related emission (with its characteristic broad peak in the range 550−630 nm) in addition to band-edge emission. The fact that the surface trap state related emission of the as-formed mixture of products arises only from NRs with size within a narrow range is of fundamental interest and is an example of the type of information that cannot be obtained without an effective means

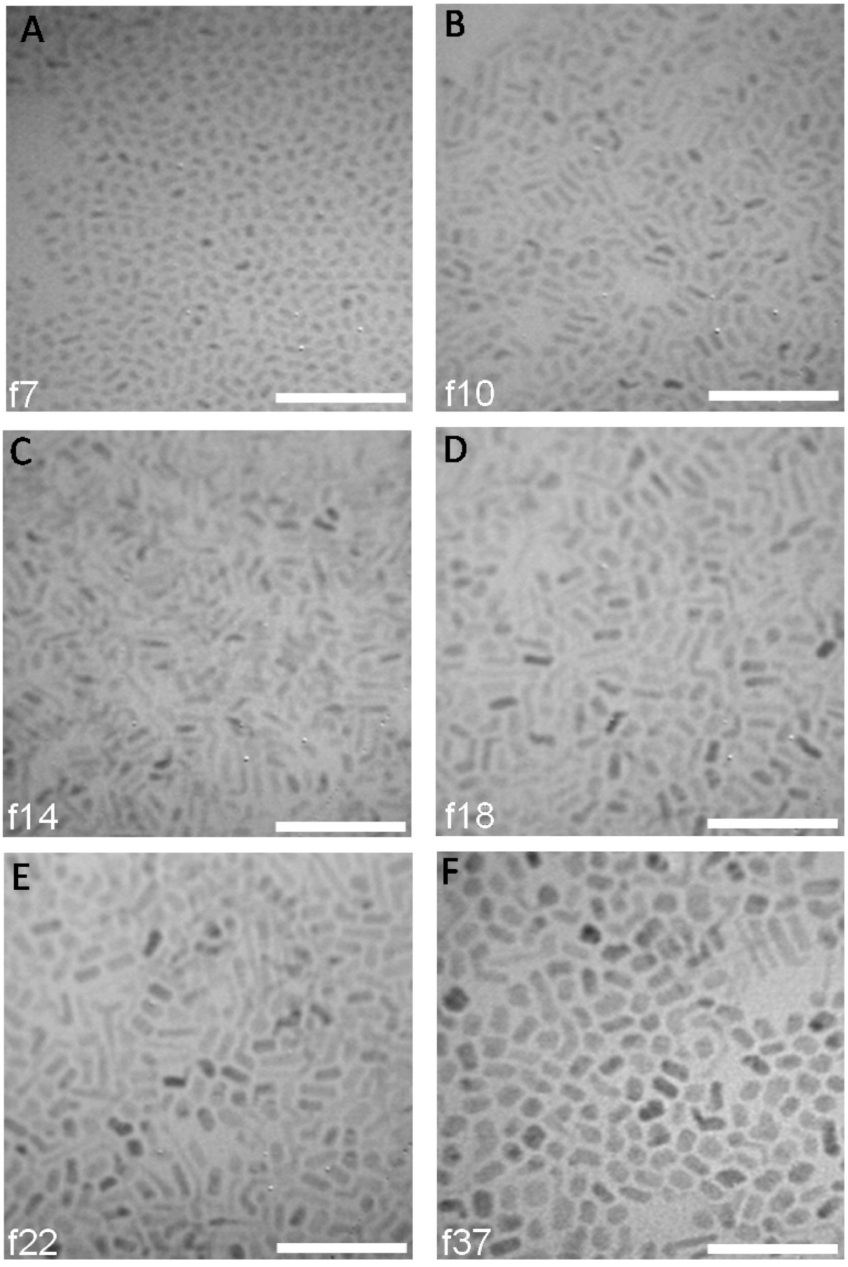

Figure 3. TEM images of CdS NR fractions separated by DGURS (the scale bar is 50 nm in each case).

of separation of nanoparticles. The absorbance spectra of the different fractions shown in Figure 2B also show a similar red-shift with increasing fraction number. The band gaps of the CdS NRs calculated from the absorbance wavelength increased from 2.72 eV (f7) to 2.46 eV (f37), which is consistent with the trend revealed by the PL emission data.

The evolution in morphology of the different NR fractions was investigated by TEM. The rods in f7 were only ~3.1 nm in diameter and ~6.8 nm in length. The rods in subsequent fractions became longer—~10 nm for f10 and ~13 nm for f14—but their diameters remained almost unchanged. Figure 2B shows that photoluminescence spectra of these fractions (f7 to f14) shifted very little (from 460 to 470 nm), suggesting that the band-edge emission of CdS NRs depends strongly on their diameter, but is less sensitive to their length;[30] similar observations have been reported for CdSe NRs.[33] The NRs in the fractions in the bottom half of the tube (from f18 to f37) showed a significant increase in diameter (from ~4.2 nm to ~6.5 nm, an increase of 55%) but only a relatively small decrease in length (from ~12.3 nm to ~10.6 nm, a decrease of 14%). For f37, which contains thick rods of diameter ~6.5 nm, only band-edge emission at 510 nm was seen, the same as that in bulk CdS. For all other fractions, blue-shifted band-edge emissions are observed (Figure 2B). This is consistent with a previous study of CdS NRs, which concluded that a diameter of ~7 nm is the threshold for showing quantum size

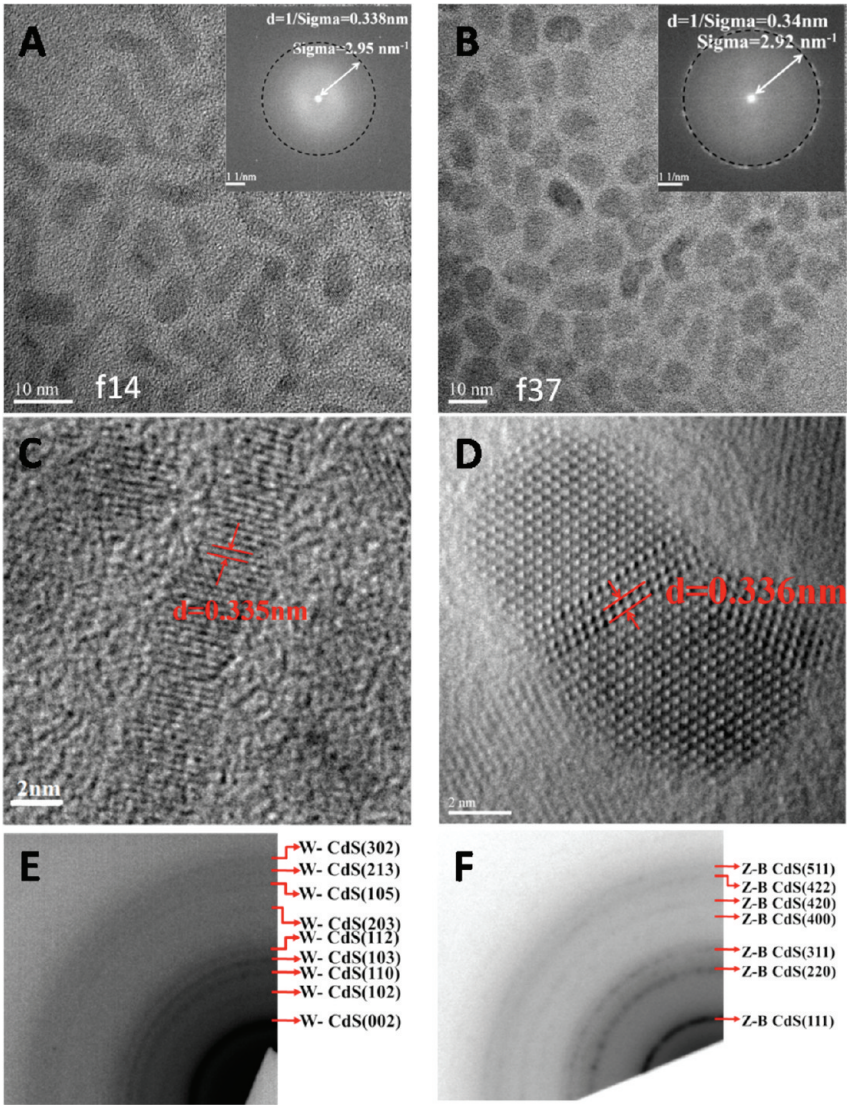

Figure 4. (A, C) HRTEM images of f14; (B, D) HRTEM images of f37 (insets: fast Fourier transform (FFT) patterns); (E, F) electron diffraction patterns of f14 and f37.

effects[22,31] and that larger NRs show essentially the same optical properties as the bulk material.

The successful separation of NR fractions provides an opportunity for further investigation of the structural differences between individual CdS NRs in each fraction, and HRTEM (high-resolution transmission electron microscopy) and ED (electron diffraction) were employed for phase identification. HRTEM images (Figure 4a and b) revealed the good crystallinity of all the NRs. NRs in all the fractions showed essentially identical characteristic lattice fringes with an interplanar spacing of 0.33 nm. This suggests that the NRs grew along the ⟨001⟩ direction when crystallized in the wurtzite phase, but along the ⟨111⟩ direction in the ZB phase because both the (111) interplanar distance of the ZB phase and the (002) interplanar distance of the wurtzite phase are 0.336 nm. Thus it is impossible to determine the phase composition or purity by simply measuring the predominant interplanar distance. However electron diffraction (Figure 4c), which gives information about more lattice planes, can be employed.

Since the XRD patterns of the wurtzite and ZB phases are very similar, the ED patterns also closely resemble one another. However, phase purity can be established by confirming the absence of diffraction spots from one of the small number of reflections that are distinctive to one polymorph or by confirming the brightness of diffraction rings. For example, the absence of the (103) diffraction ring of the wurtzite phase was taken as indicative of a pure ZB phase, while the absence of the (004) diffraction ring of the ZB phase was chosen to indicate a pure wurtzite phase. The results revealed that the phase composition of the fractions varied with the length and aspect ratio of the NRs. Because the NRs in fraction 7 were very small, the ED pattern of this material (see Supporting Information, Figure S1) showed very diffuse diffraction rings.

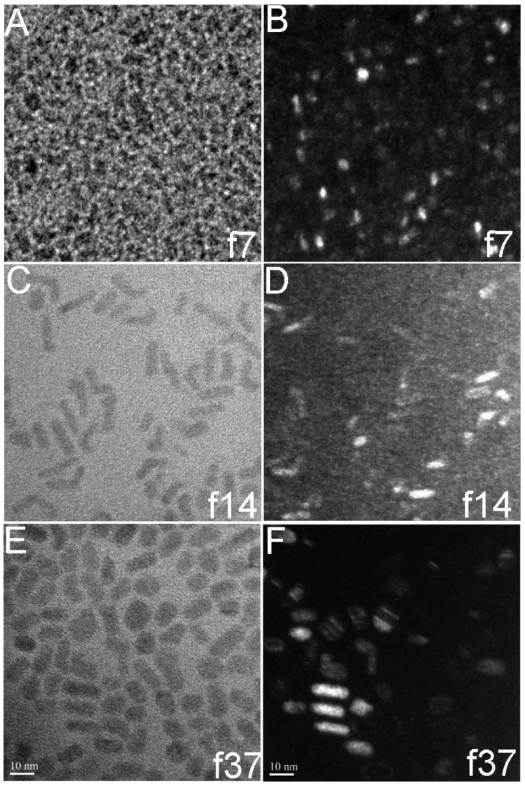

Figure 5. (A, C, E) Bright-field TEM images of f7, f14, and f37; (B, D, F) dark-field TEM images of the same samples.

However, the (103) ring could be detected, indicating that the NRs had a wurtzite structure. Fraction 14 showed a typical wurtzite phase with nine rings coinciding with the standard interplanar spacing data and no other rings. The ED pattern of fraction 37 was typical of a pure ZB phase of CdS nanocrystals; however, the diffraction ring of the (400) plane of the ZB phase was clearly seen, while the (103) diffraction ring of a wurtzite phase was absent (Figure 1B). The transition from ZB to wurtzite started at around f18, suggesting this is a mixed phase: as shown in the Supporting Information (Figure S1), the (002), (110), and (112) rings of the wurtzite phase are less sharp than for earlier fractions, suggesting overlap with the (111), (220), and (311) rings, respectively, of a ZB phase. Meanwhile, the (103) ring of the wurtzite phase was much weaker than these three rings, supporting the suggestion that a mixed phase was present. Raman was also tried on these fractions to support the phase difference, but it failed because these two phases have overlapped Raman patterns (data not shown).

The changes in the ED patterns are consistent with the PL spectra (Figure 2B), which showed a clear change in PL properties from f14 to f18. Before f14, all the samples showed a single PL peak at about 470 nm with slight red-shift as the aspect ratio increased. However, from f18 to f22, this peak became weaker and another peak at 510 nm began to increase in intensity, and thus two peaks coexisted. Finally, for f37, the lower wavelength peak disappeared, leaving a single, higher wavelength peak. Taken together with the ED results, it can be concluded that the increase in thickness and concomitant change in phase composition occurred around f18 to f22, while in the earlier fractions before f14 (d < 3.5 nm), all the samples were predominantly wurtzite phase, and the fractions near the bottom of the tube (e.g., f37, d > 5 nm) were preponderantly ZB phase.

HRTEM indicated that many of the thicker NRs had defects and showed polycrystalline structures, while the slimmer rods were mostly single crystals and had more uniform length distributions. In order to gain more statistical and direct evidence, we compared the bright-field (BF) and dark-field (DF) TEM images (Figure 5) of the samples. Single-crystal NRs should appear as the same size in BF and DF images, while polycrystalline NRs should appear smaller in a DF image than in a BF image. The rods in f7 and f14 had the same size in the two images, indicative of single crystallinity. The NRs in f37 were obviously smaller in the DF image than in the BF image, implying they are polycrystalline. Interestingly, stripes perpendicular to the longitudinal direction of the NRs were observed in the NRs in f37 having a pure ZB phase, suggesting the presence of stacking faults growing along the radical direction and perpendicular to the axial direction. Thus, NRs with the ZB phase are characterized by relatively large diameter, perpendicular stacking faults, and band-edge emission similar to bulk CdS, while those with the wurtzite phase are characterized by smaller diameters, single crystallinity, and blue-shifted band-edge emission compared with the bulk.

Since nanoseparation played an important role in revealing the structural differences between the CdS NRs and it is well-known that mathematical modeling of the separation and purification process allows the efficiency of the process to be improved,[34−36] we therefore tried to analyze details of the separation process based on histogram data after careful counting of the NRs and conclusions from analytical ultracentrifuge (AUC).[37,38] It was found that neither the length nor aspect ratio of the fractions varied monotonically from top to bottom. This indicates a different mechanism for the separation of the NR samples from that proposed for the separation by DGURS of essentially spherical nanoparticles.[28] The size of colloid particles—a combination of length and diameter—is therefore not the only factor that controls the separation, and the influence of shape should also be considered when constructing a mathematical model because differently shaped colloids have different behavior under density gradient ultracentrifugation.

At the start of the ultracentrifugation process, the NRs undergo accelerated motion in the centrifuge tube under the collective influence of the centrifugal force, buoyancy, and viscous resistance. However, the

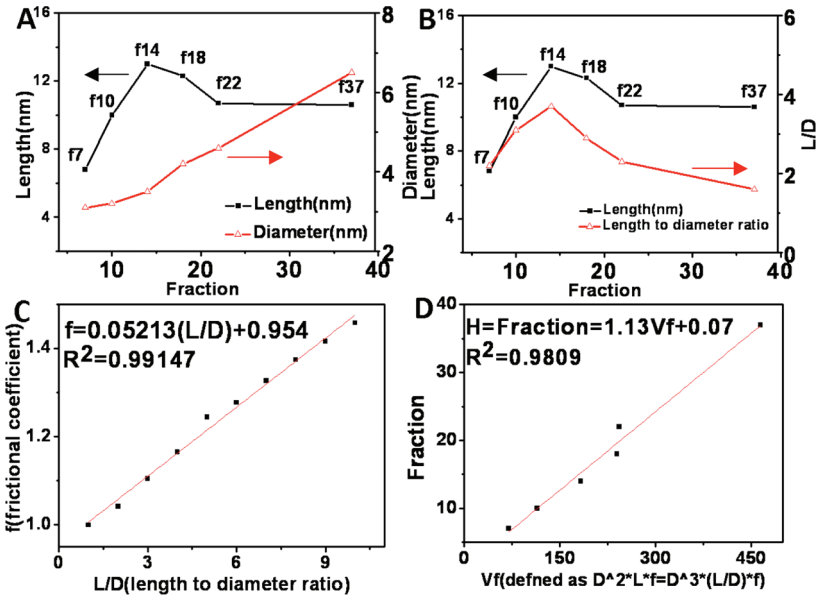

Figure 6. (A and B) Length and diameter distributions for the NR fractions; (C) frictional coefficient values and linear curve fitting of the data; (D) plot of fraction number *vs* V_f, where *D* and *L* represent the diameter and length of the NRs, and *f* represents the frictional coefficient.

acceleration process is very short-lived, and the NRs quickly reach an equilibrium state, in which they keep moving with a constant velocity.[39] According to the theory of hydromechanics, the influence of particle shape is mainly manifested in the viscous resistance when the NRs are forced to move down the centrifuge tube. Thus we corrected the viscous resistance by a frictional coefficient (defined as *f*), which results in the following equation to describe the moving state of the fraction in the process of separation:

$$\frac{d^2x}{dt^2} + f\frac{9\eta}{2\rho_p r^2}\frac{dx}{dt} + \frac{\rho_m - \rho_p}{\rho_p}\omega^2 x = 0 \qquad \textbf{(I)}$$

where *x* is the distance from the NRs to the top of the centrifuge tube, η is the viscosity of the solution, ω is the rotational speed of the centrifuge, ρ_p is the density of the NRs, and ρ_m is the density of the solution. The average density (4.85 g/cm^3) of ZB CdS (4.87 g/cm^3) and wurtzite CdS (4.82 g/cm^3) was used because the density difference between these two can be neglected when compared to the density of the medium (about 1 g/cm^3). Svedberg and Pedersen[40] have calculated different *f* values for particle length-to-diameter ratios from 1 to 10. An empirical formula can be calculated by curve fitting of their data (Figure 3C).

$$f = 0.05213(L/D) + 0.954 \qquad \textbf{(II)}$$

As the size and shape of the particles can affect the motion of NRs in the separation process, we define a parameter V_f (volume $\times$ fraction) to characterize the distribution of each fraction. Compared with plots of diameter *vs* fraction number, length *vs* fraction number, and length-to-diameter ratio *vs* fraction number, a plot of fraction number *vs* V_f exhibited a better linear correlation with the coefficient of determination *R*-squared of 0.98. Finally we obtained an empirical formula (shown below and in Figure 3D) to describe the relationship between the diameter and *L*/*D* (length-to-diameter ratio) of the particle and the location (*H* = fraction; $H \times 0.175 + 1.9$ cm corresponds to the distance between the fraction and the top of the centrifuge tube) of each fraction.

$$\begin{aligned} H = \text{fraction} &= 1.13V_f + 0.07 \\ &= 1.13D^3(L/D)[0.05213(L/D) + 0.954] + 0.07 \end{aligned} \qquad \textbf{(III)}$$

This equation verifies that not only the size but also the shape of the particles had an important influence on the separation process. This conclusion should be useful when determining the optimum experimental parameters for the separation of other anisotropic nanoparticles with rigid structures.

CONCLUSION

For the first time we have shown that the density gradient ultracentrifugation rate separation method can be used to sort CdS NRs according to differences in phase. We have also revealed the consequences of phase difference, including NR diameter, presence of defects, aspect ratio, and wavelength of band-edge photoluminescence. The discriminative separation thus provided further insight into the differences in the phase, structure, and optical properties between individual colloidal particles synthesized in a single batch. Similar experiments can be performed to reveal the structural and property differences between other colloidal nanoparticles. A preliminary mathematical

model has been established, based on histogram data of particle size, which should assist in determining the optimum parameters for the separation of other nanostructures.

EXPERIMENTAL SECTION

Reagents. All the reagents used were of analytical grade, purchased from Beijing Chemical Reagent Factory, and used as received without further purification.

Synthesis of CdS NRs (ref 21). In a typical synthesis, 0.5 mmol of $Cd(CH_3COO)_2 \cdot 2H_2O$ was added to 12.5 mL of oleylamine at room temperature, and the mixture was stirred for 30 min to form a clear solution. Then 0.6 mmol of thioacetamide was added, and the mixture was stirred for another 15 min. The solution was then transferred into a Teflon-lined autoclave (40 mL), and nitrogen was bubbled through for 1 h. The autoclave was then heated at 160 °C for 24 h. After centrifuging and washing with ethanol and cyclohexane, the as-prepared products were dispersed in cyclohexane or chloroform for characterization.

Separation of CdS NRs (refs 28, 29). All experiments were performed using a Beckman Optima L8-80M ultracentrifuge. A five-layer gradient was made of 30%, 40%, 50%, 60%, and 70% concentration solutions (by volume: cyclohexane/cyclohexane + CCl_4) was prepared in Beckman centrifuge tubes (polyallomer, inner diameter 14 mm, length 89 mm). A density gradient was created by adding layers to the tube with decreasing density (i.e., decreasing CCl_4 concentration). First 2 mL of the 70% solution was added to the centrifuge tube; then 2 mL of the 60% solution was slowly layered above the 70% layer. The subsequent layers were made following the same procedure and resulted in a density gradient along the axial direction of the centrifuge tube. Then 0.5 mL of a CdS colloid solution (~5 mg/mL) was added on top of the five-layer density gradient, and the tube was then centrifuged at 30 000 rpm for 70 min (SW-41 Ti rotor) (shown in Figure 1A). A 250 μL portion of each fraction was manually sampled for characterization.

Fluorescence Spectrophotometry. Fluorescence characterization was performed in transmission mode on a Hitachi F-4500 spectrophotometer over the range 800 to 400 nm. Measurements were performed in a 1 cm path length quartz cuvette with an excitation wavelength of 360 nm.

Absorbance Spectroscopy. The absorption spectra were measured using a Unico 2802PC absorbance spectrophotometer (200−900 nm) at room temperature.

Transmission Electron Microscopy. Transmission electron microscopy (Hitachi H-800) and high-resolution transmission electron microscopy (JEOL JEM-2100) were used to evaluate the size and shape of the nanocrystals and also for ED measurements. Samples were prepared by dropping fractions onto carbon film-supported copper grids and dried naturally. The diffraction ring nearest to the (000) spot, that is, (002) of the wurtzite phase or (111) of the ZB phase, was used for dark-field imaging.

X-ray Diffraction. X-ray diffraction patterns of samples were collected on a Shimadzu XRD-6000 diffractometer with Cu Kα radiation (40 kV, 30 mA, λ = 1.5418 Å).

Acknowledgment. This work was supported by NSFC, the 973 Program (2011CBA00503), the Foundation for Authors of National Excellent Doctoral Dissertations of P. R. China, and the Program for New Century Excellent Talents in Universities.

Supporting Information Available: HRTEM and ED patterns of fraction 7 and fraction 18 are shown in Figure S1, in which f18 could be used to explain a mix-phase structure. Figure S2 shows the raw ED patterns of each fraction. This material is available free of charge *via* the Internet at http://pubs.acs.org.

Note Added after ASAP Publication: The 973 Program number in the Acknowledgment section was incorrectly stated in the version of this paper that published ASAP on March 10, 2011. The corrected version was reposted on March 16, 2011.

REFERENCES AND NOTES

1. Kamat, P. V. Quantum Dot Solar Cells. Semiconductor Nanocrystals as Light Harvesters. *J. Phys. Chem. C* **2008,** *112*, 18737–18753.
2. Yang, H. S.; Santra, S.; Holloway, P. H. Synthesis and Applications of Mn-doped II-VI Semiconductor Nanocrystals. *J. Nanosci. Nanotechnol.* **2005,** *5*, 1364–1375.
3. Fu, A.; Gu, W. W.; Larabel, C.; Alivisatos, A. P. Semiconductor Nanocrystals for Biological Imaging. *Curr. Opin. Neurobiol.* **2005,** *15*, 568–575.
4. Huynh, W. U.; Dittmer, J. J.; Alivisatos, A. P. Hybrid Nanorod-Polymer Solar Cells. *Science* **2002,** *295*, 2425–2427.
5. Bruchez, M.; Moronne, M.; Gin, P.; Weiss, S.; Alivisatos, A. P. Semiconductor Nanocrystals as Fluorescent Biological Labels. *Science* **1998,** *281*, 2013–2016.
6. Chan, W. C. W.; Nie, S. M. Quantum Dot Bioconjugates for Ultrasensitive Nonisotopic Detection. *Science* **1998,** *281*, 2016–2018.
7. Colvin, V. L.; Schlamp, M. C.; Alivisatos, A. P. Light-emitting Diodes Made from Cadmium Selenide Nanocrystals and a Semiconducting Polymer. *Nature* **1994,** *370*, 354–357.
8. Tessler, N.; Medvedev, V.; Kazes, M.; Kan, S.; Banin, U. Efficient Near-Infrared Polymer Nanocrystal Light-Emitting Diodes. *Science* **2002,** *295*, 1506–1508.
9. Coe, S.; Woo, W.-K.; Bawendi, M.; Bulovic, V. Electroluminescence from Single Monolayers of Nanocrystals in Molecular Organic Devices. *Nature* **2002,** *420*, 800–803.
10. Huang, Y.; Lieber, C. M. Integrated Nnanoscale Electronics and Optoelectronics: Exploring Nanoscale Science and Technology Through Semiconductor Nanowires. *Pure Appl. Chem.* **2004,** *76*, 2051–2068.
11. Klimov, V. I.; Mikhailovsky, A. A.; Xu, S.; Malko, A.; Hollingsworth, J. A.; Leatherdale, C. A.; Eisler, H. J.; Bawendi, M. G. Optical Gain and Stimulated Emission in Nanocrystal Quantum Dots. *Science* **2000,** *290*, 314–317.
12. Kazes, M.; Lewis, D. Y.; Ebenstein, Y.; Mokari, T.; Banin, U. Lasing from Semiconductor Quantum Rods in a Cylindrical Microcavity. *Adv. Mater.* **2002,** *14*, 317–321.
13. Bai, F.; Wang, D. S.; Huo, Z. Y.; Chen, W.; Liu, L. P.; Liang, X.; Chen, C.; Wang, X.; Peng, Q.; Li, Y. D. A Versatile Bottom-up Assembly Approach to Colloidal Spheres from Nanocrystals. *Angew. Chem., Int. Ed.* **2007,** *119*, 6770–6773.
14. Xiong, S. L.; Zhang, X. Z.; Qian, Y. T. CdS with Various Novel Hierarchical Nanostructures by Nanobelts/Nanowires Self-Assembly: Controllable Preparation and Their Optical Properties. *Cryst. Growth Des.* **2009,** *9*, 5259–5265.
15. Yao, W. T.; Yu, S. H.; Liu, S. J.; Chen, J. P.; Liu, X. M.; Li, F. Q. Architectural Control Synthesis of CdS and CdSe Nanoflowers, Branched Nanowires, and Nanotrees via a Solvothermal Approach in a Mixed Solution and Their Photocatalytic Property. *J. Phys. Chem. B* **2006,** *110*, 11704–11710.
16. Chen, M.; Xie, Y.; Lu, J.; Xiong, Y. J.; Zhang, S. Y.; Qian, Y. T.; Liu, X. M. Synthesis of Rod-, Twinrod-, and Tetrapod-shaped CdS Nanocrystals Using a Highly Oriented Solvothermal Recrystallization Technique. *J. Mater. Chem.* **2002,** *12*, 748–753.
17. Chu, H. B.; Ding, L.; Wang, J. Y.; Li, X. M.; You, L. P.; Li, Y. In Situ Epitaxial Growth of Triangular CdS Nanoplates on Mica by Dip-Pen Nanolithography. *J. Phys. Chem. C* **2008,** *112*, 18938–18942.
18. Chu, H. B.; Li, X. M.; Chen, G. D.; Zhou, W. W.; Zhang, Y.; Jin, Z.; Xu, J. J.; Li, Y. Shape-controlled Synthesis of CdS Nanocrystals in Mixed Solvents. *Cryst. Growth Des.* **2005,** *5*, 1801–1806.
19. Li, Y. C.; Li, X. H.; Yang, C. H.; Li, Y. F. Controlled Synthesis of CdS Nanorods and Hexagonal Nanocrystals. *J. Mater. Chem.* **2003,** *13*, 2641–2648.

20. Li, Y. D.; Liao, H. W.; Ding, Y.; Qian, Y. T.; Yang, L.; Zhou, G. E. Nonaqueous Synthesis of CdS Nanorod Semiconductor. *Chem. Mater.* **1998,** *10*, 2301–2303.
21. Li, P.; Wang, L. Y.; Wang, L.; Li, Y. D. Controlled Synthesis and Luminescence of Semiconductor Nanorods. *Chem.—Eur. J.* **2008,** *14*, 5951–5956.
22. Peng, Z. A.; Peng, X. G. Formation of High-Quality CdTe, CdSe, and CdS Nanocrystals Using CdO as Precursor. *J. Am. Chem. Soc.* **2001,** *123*, 183–184.
23. Guo, Y.; Zhang, H.; Wang, Y.; Liao, Z. L.; Li, G. D.; Chen, J. S. Controlled Growth and Photocatalytic Properties of CdS Nanocrystals Implanted in Layered Metal Hydroxide Matrixes. *J. Phys. Chem. B* **2005,** *109*, 21602–21607.
24. Arnold, M. S.; Green, A. A.; Hulvat, J. F.; Stupp, S. I.; Hersam, M. C. Sorting Carbon Nanotubes by Electronic Structure Using Density Differentiation. *Nat. Nanotechnol.* **2006,** *1*, 60–65.
25. Jamison, J. A.; Krueger, K. M.; Yavuz, C. T.; Mayo, J. T.; LeCrone, D.; Redden, J. J.; Colvin, V. L. Size-Dependent Sedimentation Properties of Nanocrystals. *ACS Nano* **2008,** *2*, 311–319.
26. Fagan, J. A.; Becker, M. L.; Chun, J.; Hobbie, E. K. Length Fractionation of Carbon Nanotubes Using Centrifugation. *Adv. Mater.* **2008,** *20*, 1609–1613.
27. Chen, G.; Wang, Y.; Tan, L. H.; Yang, M. X.; Tan, L. S.; Chen, Y.; Chen, H. Y. High-Purity Separation of Gold Nanoparticle Dimers and Trimers. *J. Am. Chem. Soc.* **2009,** *131*, 4218–4219.
28. Bai, L.; Ma, X. J.; Liu, J. F.; Sun, X. M.; Zhao, D. Y.; Evans, D. G. Rapid Separation and Purification of Nanoparticles in Organic Density Gradients. *J. Am. Chem. Soc.* **2010,** *132*, 2333–2337.
29. Sun, X. M.; Tabakman, S. M.; Seo, W.-S.; Zhang, L.; Zhang, G. Y.; Sherlock, S.; Bai, L.; Dai, H. J. Separation of Nanoparticles in a Density Gradient: FeCo@C and Gold Nanocrystals. *Angew. Chem., Int. Ed.* **2009,** *48*, 939–942.
30. Sun, X. M.; Ma, X. J.; Bai, L.; Liu, J. F.; Chang, Z.; Evans, D. G.; Duan, X.; Wang, J.; Chiang, J. F. Nanoseparation-Inspired Manipulation of the Synthesis of CdS Nanorods. *Nano Res.* **2011,** *4*, 226–232.
31. Yu, W. W.; Peng, X. G. Formation of High-Quality CdS and Other II—VI Semiconductor Nanocrystals in Noncoordinating Solvents: Tunable Reactivity of Monomers. *Angew. Chem., Int. Ed.* **2002,** *41*, 2368–2371.
32. Zhuang, Z. B.; Lu, X. T.; Peng, Q.; Li, Y. D. Direct Synthesis of Water-Soluble Ultrathin CdS Nanorods and Reversible Tuning of the Solubility by Alkalinity. *J. Am. Chem. Soc.* **2010,** *132*, 1819–1821.
33. Li, L. S.; Hu, J. T.; Yang, W. D.; Alivisatos, A. P. Band Gap Variation of Size- and Shape-Controlled Colloidal CdSe Quantum Rods. *Nano Lett.* **2001,** *1*, 349–351.
34. Vauthier, C.; Schmidt, C.; Couvreur, P. Measurement of the Density of Polymeric Nanoparticulate Drug Carriers by Isopycnic Centrifugation. *J. Nanopart. Res.* **1999,** *1*, 411–418.
35. Lechner, M. D.; Machtle, W. Determination of the Particle Size Distribution of 5—100-nm Nanoparticles with the Analytical Ultracentrifuge: Consideration and Correction of Diffusion Effects. *Prog. Colloid Polym. Sci.* **1999,** *113*, 37–43.
36. Hanauer, M.; Pierrat, S.; Zins, I.; Lotz, A.; Sonnichsen, C. Separation of Nanoparticles by Gel Electrophoresis According to Size and Shape. *Nano Lett.* **2007,** *7*, 2881–2885.
37. Colfen, H.; Volkel, A. Analytical Ultracentrifugation in Colloid Chemistry. *Progr. Colloid Polym. Sci.* **2004,** *127*, 31–47.
38. Lees, E. E.; Nguyen, T.-L.; Clayton, A. H. A.; Mulvaney, P. The Preparation of Colloidally Stable, Water-Soluble, Biocompatible, Semiconductor Nanocrystals with a Small Hydrodynamic Diameter. *ACS Nano* **2009,** *3*, 1121–1128.
39. Rickwood, D.; Ford, T.; Steensgaard, J. *Centrifugation: Essential Data*; John Wiley & Sons: New York, 1994.
40. Svedberg, T.; Pedersen, K. O. *The Ultracentrifuge*; Oxford Univ. Press: Oxford, 1940.